Cdk1 phosphorylates SPAT-1/Bora to trigger PLK-1 activation and drive mitotic entry in *C. elegans* embryos

Nicolas Tavernier,[1]* Anna Noatynska,[3]* Costanza Panbianco,[3] Lisa Martino,[1] Lucie Van Hove,[1] Françoise Schwager,[3] Thibaut Léger,[2] Monica Gotta,[3,4] and Lionel Pintard[1]

[1]Jacques Monod Institute, UMR7592; and [2]Mass Spectrometry Facility, Jacques Monod Institute, UMR7592; Paris-Diderot University–Centre National de la Recherche Scientifique, 75013 Paris, France
[3]Department of Cellular Physiology and Metabolism, Faculty of Medicine, University of Geneva, CH-1211 Geneva 4, Switzerland
[4]Swiss National Centre for Competence in Research Program Chemical Biology, 1211 Geneva, Switzerland

The molecular mechanisms governing mitotic entry during animal development are incompletely understood. Here, we show that the mitotic kinase CDK-1 phosphorylates Suppressor of Par-Two 1 (SPAT-1)/Bora to regulate its interaction with PLK-1 and to trigger mitotic entry in early *Caenorhabditis elegans* embryos. Embryos expressing a SPAT-1 version that is nonphosphorylatable by CDK-1 and that is defective in PLK-1 binding in vitro present delays in mitotic entry, mimicking embryos lacking SPAT-1 or PLK-1 functions. We further show that phospho–SPAT-1 activates PLK-1 by triggering phosphorylation on its activator T loop in vitro by Aurora A. Likewise, we show that phosphorylation of human Bora by Cdk1 promotes phosphorylation of human Plk1 by Aurora A, suggesting that this mechanism is conserved in humans. Our results suggest that CDK-1 activates PLK-1 via SPAT-1 phosphorylation to promote entry into mitosis. We propose the existence of a positive feedback loop that connects Cdk1 and Plk1 activation to ensure a robust control of mitotic entry and cell division timing.

Introduction

Regulation of cell cycle duration is crucial for the development of multicellular organisms. The first embryonic division of the *Caenorhabditis elegans* (*C.e.*) embryo is asymmetric and generates two blastomeres (AB and P1) of different sizes and developmental potentials that divide asynchronously (Deppe et al., 1978; Sulston et al., 1983). This asynchrony of cell division can be easily monitored by time-lapse differential interference contrast (DIC) microscopy, which makes this embryo an ideal system to study the pathways regulating the timing of mitotic entry in a developmental context.

Mitosis is triggered by the concerted action of several conserved mitotic kinases, notably the CyclinB/Cdk1 and members of Polo-like families (Archambault and Glover, 2009). *C.e.* PLK-1, similar to all Polo-like kinase family members, is characterized by an N-terminal kinase domain and a C-terminal noncatalytic region containing two tandem Polo boxes (Polo box domain [PBD]), which recognize phosphorylated peptides (Polo docking sites; Elia et al., 2003a,b; Nishi et al., 2008).

Like other family members, PLK-1 localizes at centrosomes and at kinetochores, but it is also enriched in the anterior cytoplasm in one-cell embryos and therefore becomes preferentially segregated to the AB cell in two-cell embryos (Chase et al., 2000; Budirahardja and Gönczy, 2008; Nishi et al., 2008; Rivers et al., 2008). The higher levels of PLK-1 in AB compared with P1 promote faster nuclear import of CDC-25.1, the CDK-1–activating phosphatase, and trigger earlier mitotic entry in AB compared with P1 (Rivers et al., 2008).

A regulator of Plk1 activity is the conserved protein Bora. Bora was originally identified in *Drosophila melanogaster* and was shown to activate Aurora A (Hutterer et al., 2006). In human cells (Macůrek et al., 2008; Seki et al., 2008) and in *C.e.* (Noatynska et al., 2010), Bora/Suppressor of Par-Two 1 (SPAT-1) was reported to function as a Plk1 activator. In human cells, Bora binds Plk1 and enhances Aurora A–mediated T-loop
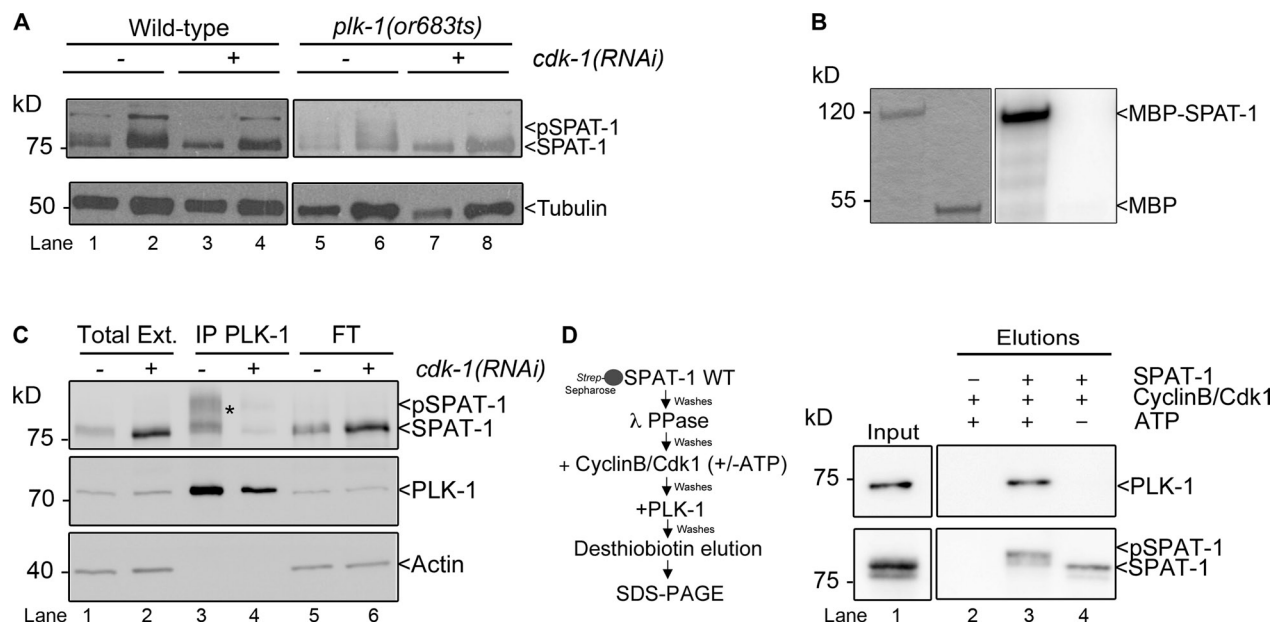
THE JOURNAL OF CELL BIOLOGY

Figure 1. **SPAT-1 phosphorylation by Cdk1 promotes the interaction between SPAT-1 and PLK-1.** (A, top) Embryonic extracts of the indicated genotypes analyzed by Western blotting using SPAT-1 antibodies. (bottom) Tubulin is used as a loading control. 25 µg (lanes 1, 3, 5, and 7) and 50 µg (lanes 2, 4, 6, and 8) of each protein extract were loaded to visualize the modified forms. (B) MBP–SPAT-1 or MBP incubated with CyclinB/Cdk1 kinase in the presence of γ-[^{32}P]ATP. (right) Autoradiograph of the SDS-PAGE gel showing ^{32}P incorporation in MBP–SPAT-1 but not MBP. (left) Coomassie staining of the same SDS-PAGE gel. (C) Western blot analysis of PLK-1 immunoprecipitates (IP PLK-1) from control (lane 3) or *cdk-1(RNAi)* (lane 4) embryonic extracts analyzed with SPAT-1 (top) and PLK-1 antibodies (middle). (bottom) Actin was used as a loading control. 10 µg (1:40) of the total extracts (Ext.; lanes 1 and 2) and the flow through (FT) of the immunoprecipitates (lanes 5 and 6) were loaded for comparison. The asterisk marks the phosphorylated SPAT-1 forms that are present in the PLK-1 immunoprecipitation. (D) In vitro assay used to test Cdk1 dependency of the interaction between SPAT-1 and PLK-1. On the left, we show a flow chart describing the assay; on the right, we show the Western blot analysis. Strep–SPAT-1 protein produced in insect Sf9 cells was immobilized on Strep-Tactin Sepharose beads, dephosphorylated with λ phosphatase (λ PPase), and incubated with CylinB/Cdk1 in the presence (+) or absence (−) of ATP. After washing the kinase and ATP, full-length 6×(His)–PLK-1 was added (+) for a typical pull-down experiment. (right) Strep–SPAT-1 was eluted with desthiobiotin, and the elutions were analyzed by SDS-PAGE and Western blotting using PLK-1 and SPAT-1 antibodies.

phosphorylation of Plk1, which is critical for full Plk1 activation (Macůrek et al., 2008; Seki et al., 2008).

Although SPAT-1/Bora is required for Plk1 activation, the regulation of the interaction between SPAT-1/Bora and Plk1 is unclear (Bruinsma et al., 2012). Here, we find that CDK-1 phosphorylates SPAT-1 to regulate its interaction with PLK-1 and to enhance Aurora A–mediated T-loop phosphorylation of PLK-1 in vitro. Mutations that mimic the nonphosphorylatable forms of SPAT-1 strongly impair mitotic entry time of early *C.e.* embryos. We also show that the phosphorylation of human Bora by Cdk1 similarly enhances T-loop phosphorylation of human Plk1 by Aurora A. Overall, our results suggest a model in which SPAT-1/Bora is part of a positive feedback loop that coordinates PLK-1 and CDK-1 activation for timely mitotic entry.

Results and discussion

Phosphorylation of SPAT-1 depends on Cdk1

SPAT-1 is a phosphoprotein modified at multiple residues observed as slower migrating bands on 1D gel separation (Fig. 1 A, lanes 1 and 2; Noatynska et al., 2010). Given that SPAT-1 is a PLK-1 substrate (Noatynska et al., 2010), these forms could correspond to species phosphorylated by PLK-1. However, SPAT-1–phosphorylated forms accumulated in *plk-1* temperature-sensitive mutant embryos and in PLK-1–depleted embryos

(Fig. 1 A, lanes 5 and 6; Noatynska et al., 2010), indicating that at least another kinase phosphorylates SPAT-1 in vivo.

Human Bora is phosphorylated in mitosis, and both Plk1 and CyclinB/Cdk1 phosphorylate Bora in vitro (Hutterer et al., 2006; Chan et al., 2008). Similar to Bora, SPAT-1 contains multiple minimal CDK consensus sites ((S/T)-P). We thus investigated whether CDK-1 phosphorylates SPAT-1. Weak inactivation of *cdk-1* in wild-type (WT) embryos resulted in a reduction of SPAT-1 phosphorylation (Fig. 1 A, compare lanes 1 and 2 with 3 and 4). Likewise, inactivation of *cdk-1* in the *plk-1(or683)* temperature-sensitive mutant suppressed the accumulation of the hyperphosphorylated forms of SPAT-1 (Fig. 1 A, compare lanes 5 and 6 with 7 and 8), indicating that some of the phosphorylated SPAT-1 species are CDK-1 dependent. We then tested whether CDK-1 can phosphorylate SPAT-1 in vitro. CyclinB/Cdk1 phosphorylated Maltose-binding protein (MBP)–SPAT-1 but not the MBP control (Fig. 1 B). Therefore, SPAT-1 is phosphorylated by CDK-1 in vitro and in a CDK-1–dependent manner in vivo.

Phosphorylation of SPAT-1 by CDK-1 promotes its interaction with PLK-1

Phosphorylated forms of SPAT-1 are enriched in PLK-1 immunoprecipitates (Fig. 1 C, lane 3; Noatynska et al., 2010) and a reduced fraction of phospho–SPAT-1 was recovered in the PLK-1 immunoprecipitation from embryos with partial *cdk-1(RNAi)* (Fig. 1 C, compare lanes 3 and 4, the pSPAT-1/PLK-1 ratio
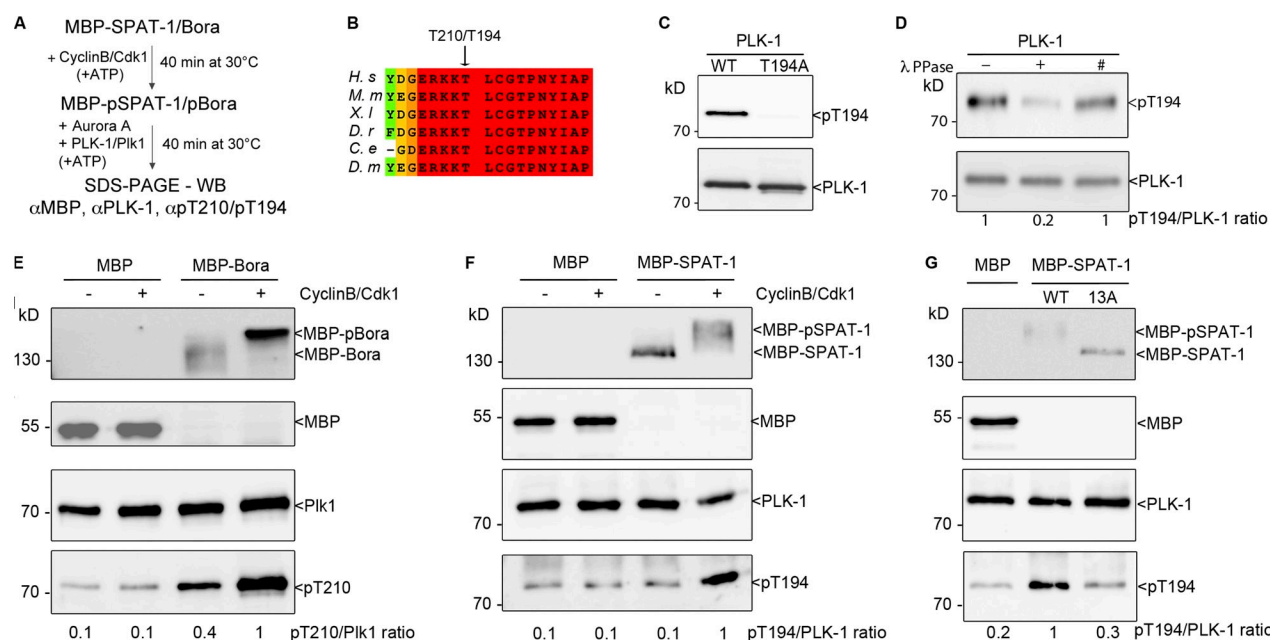
Figure 2. **CyclinB/Cdk1 phosphorylates SPAT-1 at multiple sites.** (A) Flow chart of the approach used to map SPAT-1 phosphorylation sites in vitro and in vivo. IP, immunoprecipitation. LC-MS/MS, tandem MS. (B) Table showing the amino acid position of the CDK-1–dependent phosphorylation sites in SPAT-1 protein sequence (F57C2.6b) with the 13 (S/T)p sites identified in vitro (highlighted in light gray), seven of which were confirmed in vivo (highlighted in dark gray). (C) Kinase assay conducted with purified Strep–SPAT-1 WT or Strep–SPAT-1 13A with human CyclinB/Cdk1 and γ-[^{32}P]ATP. (top) SDS-PAGE gel stained with Coomassie shows protein loading. (bottom) Autoradiography indicates SPAT-1 phosphorylation status. (D) Strep pull-downs from insect Sf9 cells coexpressing PLK-1 and Strep–SPAT-1 WT (lanes 1 and 4), PLK-1 and SPAT-1 13A mutant (lanes 2 and 5), or PLK-1 alone (lanes 3 and 6) were analyzed by SDS-PAGE and probed with PLK-1 (top) and SPAT-1 (bottom) antibodies. A fraction (1/100) of the total protein extracts (Total) was loaded in the lanes 1–3. (E) Strep–SPAT-1 WT or the nonphosphorylatable 13A mutant version was immobilized on Strep-Tactin Sepharose beads, phosphorylated by CyclinB/Cdk1, and incubated with PLK-1 for pull-down experiments. The SPAT-1–PLK-1 complex was eluted with desthiobiotin (Elutions) and analyzed by SDS-PAGE. The membrane was blotted with PLK-1 (top) and SPAT-1 antibodies (bottom). (F) Western blot showing the result of the gel filtration analysis of Strep–SPAT-1 WT (top) and Strep–SPAT-1 13A (bottom) proteins. The proteins used to calibrate the column are indicated on the top.

	S36	T57	T78	S119	S190	T229	S251	T328	S368	T456	T465	S504	T518
In vitro	■	■	■	■	■	■	■	■	■	■	■	■	■
In vivo	■	■			■	■	■	■				■	

decreased from 1 in control to 0.2 in *cdk-1(RNAi)* embryos), suggesting that CDK-1 might phosphorylate SPAT-1 to promote its interaction with PLK-1. To test this hypothesis, we developed an in vitro binding assay (Fig. 1 D) in which full-length Strep–SPAT-1 produced in insect *Spodoptera frugiperda* 9 (Sf9) cells was immobilized on Strep-Tactin Sepharose beads. CyclinB/Cdk1 was added in the presence or absence of ATP (±ATP) to trigger SPAT-1 phosphorylation. CyclinB/Cdk1 kinase was washed away, and immobilized SPAT-1 or phospho (p)–SPAT-1 was incubated with PLK-1 for pull-down experiments. As shown in Fig. 1 D, pSPAT-1 (incubated with CyclinB/Cdk1 and ATP) pulled down PLK-1 (Fig. 1 D, lane 3) as compared with the nonphosphorylated version (Fig. 1 D, lane 4, incubated with the kinase but without ATP) consistent with the in vivo finding that hyperphosphorylated forms of SPAT-1 coimmunoprecipitate with PLK-1. These results indicate that CyclinB/Cdk1-dependent phosphorylation of SPAT-1 promotes its interaction with PLK-1.

CDK-1 phosphorylates SPAT-1 at multiple sites

To identify the residues phosphorylated by CDK-1, we subjected SPAT-1, phosphorylated in vitro by human CyclinB/Cdk1, to tandem mass spectrometry (MS; liquid chromatography [LC]–MS/MS) analysis and identified 13 ((S/T)P) residues (S36, T57, T78, S119, S190, T229, S251, T328, S368, T456, T465, S504, and T518; Fig. 2, A and B; and Table S2). A nonphosphorylatable SPAT-1^{13A} mutant (with all S and T of the (S/T)P sites mutated to alanine) displayed a significantly dampened phosphorylation by CyclinB/Cdk1 (Fig. 2 C), indicating that these 13 residues are indeed the major CyclinB/Cdk1 phosphorylation sites. MS analysis of endogenous SPAT-1 or GFP::SPAT-1 immunoprecipitated from WT embryonic extracts confirmed that SPAT-1 is phosphorylated in vivo on at least 7 (S36, T57, S190, T229, S251, T328, and S504) out of the 13 residues that are phosphorylated by Cdk1 in vitro (Materials and methods; Fig. 2 B and Table S2).

We next asked whether SPAT-1 phosphorylation on these sites regulates its interaction with PLK-1. We coexpressed Strep–SPAT-1 WT or Strep–SPAT-1 13A mutant with 6×(His)–PLK-1 in insect Sf9 cells and performed a Strep pull-down experiments. SPAT-1 WT, but not the SPAT-1 13A version, coprecipitated PLK-1 (Fig. 2 D, compare lanes 4 and 5). We corroborated these observations using our in vitro assay and found that the SPAT-1 13A mutant was not able to bind PLK-1 in a Cdk1-dependent manner in vitro (Fig. 2 E, lanes 1 and 2). This lack of interaction is not caused by the overall misfolding

Figure 3. **Phospho–SPAT-1 and phospho-Bora promote PLK-1/Plk1 phosphorylation on its activator T loop by the Aurora A kinase.** (A) Flow chart of the assay used to test the role of Bora/SPAT-1 phosphorylation by CyclinB/Cdk1 in Plk1 phosphorylation by Aurora A. (B) The T loop of Plk1 is evolutionarily conserved. Sequence alignment of the T-loop region of Plk1 from various species, using PRALINE (*H. s, H. sapiens; M. m, Mus musculus; X. l, X. laevis; D. r, Danio rerio; C. e, C. elegans; D. m, D. melanogaster*). Invariant residues are highlighted in red. An arrow marks the activating T210 phosphorylation of human Plk1, which corresponds to T194 in *C.e.* PLK-1. (C) Western blot of WT and T194A 6×(His)–PLK-1 mutant purified from insect Sf9 cells with the anti-Plk1 pT210 (top) and PLK-1 antibody (bottom). (D) The phospho-specific T210 Plk1 antibody specifically recognizes pT194 in *C.e.* PLK-1. 6×(His)–PLK-1 WT purified from insect Sf9 cells was incubated with λ phosphatase (λ PPase, +) or heat-inactivated phosphatase (#) and analyzed by SDS-PAGE and Western blotting using the anti-Plk1 phospho-T210 (top) and PLK-1 antibodies (bottom). (E) Western blot showing the result of the kinase assay of 6×(His)-Plk1 by 6×(His)–Aurora A incubated with MBP (lanes 1 and 2) or MBP-Bora (lanes 3 and 4) phosphorylated (+) or not phosphorylated (−) by CyclinB/Cdk1. Blots were probed with MBP (top), anti-pT210 (bottom), and Plk1 (middle) antibodies. (F) Western blot showing the result of the kinase assay of 6×(His)–PLK-1 by 6×(His)–Aurora A incubated with MBP (lanes 1 and 2) or MBP–SPAT-1 (lanes 3 and 4) phosphorylated (+) or not phosphorylated (−) by CyclinB/Cdk1. Blots were probed with MBP (top), anti-pT210 (bottom), and Plk1 (middle) antibodies. (G) Western blot showing the result of the kinase assay of 6×(His)–PLK-1 by 6×(His)–Aurora A incubated with MBP (lane 1), MBP–SPAT-1 WT (lane 2), or MBP–SPAT-1 13A mutant phosphorylated by CyclinB/Cdk1. Blots were probed with MBP (top), anti-pT210 (bottom), and PLK-1 (middle) antibodies.

and aggregation of the SPAT-1 13A mutated protein because SPAT-1 13A was fully soluble in our extraction conditions and did not elute in the void volume in gel filtration experiments (Fig. 2 F). Collectively, these results indicate that SPAT-1 phosphorylation by CDK-1 regulates its interaction with PLK-1.

SPAT-1 phosphorylation stimulates Aurora A–dependent phosphorylation of PLK-1 on its activator T loop

In human cells, Bora has been suggested to trigger Plk1 activation by promoting its phosphorylation on the T loop (residue T210) by Aurora A at the G2/M cell cycle transition (Macůrek et al., 2008; Seki et al., 2008). At this transition, Bora is highly phosphorylated (Chan et al., 2008; Seki et al., 2008), raising the hypothesis that Bora phosphorylation might stimulate Aurora A activity toward Plk1.

To test this, we developed an in vitro assay that specifically monitors the activity of Aurora A toward *Homo sapiens* (*H.s.*) Plk1/*C.e.* PLK-1 in the presence of *H.s.* Bora/*C.e.* SPAT-1, phosphorylated or not by CyclinB/Cdk1 (Fig. 3 A and S1). We used a phosphospecific antibody that recognizes phosphorylated Threonine 210 of *H.s.* Plk1 and the equivalent phosphorylated residue in *C.e.* PLK-1 (T194; Fig. 3, B–D). Consistent with previous studies (Macůrek et al., 2008; Seki et al., 2008),

nonphosphorylated MBP-Bora was able to stimulate human Plk1 phosphorylation on the T loop by Aurora A in vitro (Fig. 3 E). However, this effect was enhanced when MBP-Bora was pre-phosphorylated by Cdk1 (Fig. 3 E), indicating that Bora phosphorylation by Cdk1 stimulates human Plk1 phosphorylation by Aurora A.

We next tested whether phosphorylation of *C.e.* SPAT-1 by Cdk1 similarly stimulates *C.e.* PLK-1 phosphorylation by Aurora A. As shown in Fig. 3 F, the activity of Aurora A toward *C.e.* PLK-1 was not enhanced by the addition of the MBP control or nonphosphorylated MBP–SPAT-1. However, addition of MBP–SPAT-1 phosphorylated by Cdk1 stimulated *C.e.* PLK-1 phosphorylation at T194 by Aurora A (Fig. 3 F), whereas the nonphosphorylatable SPAT-1 13A mutant was defective in promoting PLK-1 phosphorylation by Aurora A (Fig. 3 G). We conclude that phosphorylation of both *C.e.* SPAT-1 and human Bora by Cdk1 stimulates phosphorylation of PLK-1 at the T loop by Aurora A.

Contribution of CDK-1 phosphorylation sites to SPAT-1 function in vivo

To analyze the role of SPAT-1 phosphorylation in vivo, we generated lines expressing *GFP::spat-1* RNAi-resistant transgenes (hereafter, *GFP::spat-1*[R]) WT or with different combination of
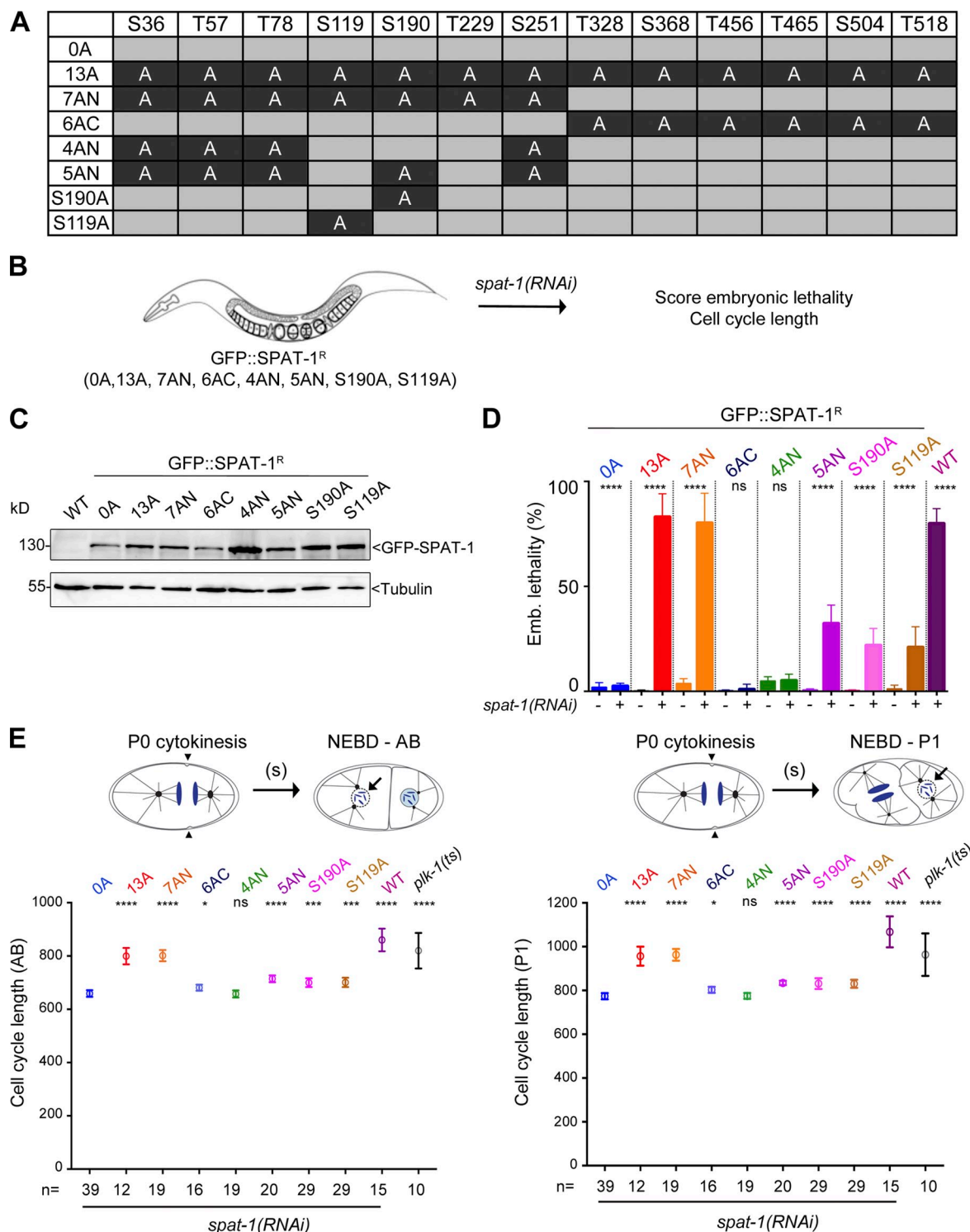
A

	S36	T57	T78	S119	S190	T229	S251	T328	S368	T456	T465	S504	T518
0A													
13A	A	A	A	A	A	A	A	A	A	A	A	A	A
7AN	A	A	A	A	A	A	A						
6AC								A	A	A	A	A	A
4AN	A	A	A				A						
5AN	A	A	A		A		A						
S190A					A								
S119A				A									

B

spat-1(RNAi) → Score embryonic lethality / Cell cycle length

GFP::SPAT-1^R
(0A, 13A, 7AN, 6AC, 4AN, 5AN, S190A, S119A)

C

GFP::SPAT-1^R

kD — WT, 0A, 13A, 7AN, 6AC, 4AN, 5AN, S190A, S119A

130 — <GFP-SPAT-1
55 — <Tubulin

D

GFP::SPAT-1^R

Emb. lethality (%)

0A, 13A, 7AN, 6AC, 4AN, 5AN, S190A, S119A, WT

spat-1(RNAi) − +

**** **** **** ns ns **** **** **** ****

E

P0 cytokinesis → (s) → NEBD - AB

0A, 13A, 7AN, 6AC, 4AN, 5AN, S190A, S119A, WT, plk-1(ts)

**** **** * ns **** *** *** **** ****

Cell cycle length (AB)

n= 39 12 19 16 19 20 29 29 15 10

spat-1(RNAi)

P0 cytokinesis → (s) → NEBD - P1

0A, 13A, 7AN, 6AC, 4AN, 5AN, S190A, S119A, WT, plk-1(ts)

**** **** * ns **** **** **** **** ****

Cell cycle length (P1)

n= 39 12 19 16 19 20 29 29 15 10

spat-1(RNAi)

Figure 4. **SPAT-1 phosphorylation at the N-terminal part is essential in vivo.** (A) Summary table presenting the SPAT-1 mutants analyzed in vivo. Sp/Tp sites mutated into alanine residues are highlighted in dark gray. (B) Schematic of the approach used to analyze the role of SPAT-1 phosphorylation in vivo. Transgenic *C.e.* lines expressing RNAi-resistant SPAT-1 (SPAT-1^R) WT (0A) or mutated on different phosphorylation sites were generated. Endogenous *spat-1* was depleted by injecting dsRNA in the different lines to measure embryonic lethality and embryonic cell cycle length in AB and P1 blastomeres. (C) Western blot analysis of embryos expressing *GFP*::*spat-1*^R transgenes using SPAT-1 (top) and Tubulin (loading control; bottom) antibodies. (D) Graph showing the percentage of lethality of embryos (Emb.) from animals of the indicated genotype after RNAi-mediated depletion of endogenous *spat-1*. Error bars indicate 95% confidence limits. (E, top) Schematic of the first and second cell divisions of early *C.e.* embryos. DNA is in blue, and black arrows show nuclear envelope breakdown (NEBD) in AB and P1 blastomeres, which is apparent by loss of the smooth line corresponding to the nuclear envelope. The mean elapsed time in seconds between ingression of the cytokinesis furrow (black arrowheads) in P0 (P0 cytokinesis) and NEBD in AB (NEBD-AB; left) or P1 (NEBD-P1; right) was determined and plotted in embryos of the indicated genotypes (shown at the bottom). Cell cycle timing was similarly measured in *plk-1(or689*ts) embryos for comparison. Error bars indicate 95% confidence limits, and asterisks denote a statistically significant difference: ****, P < 0.0001; ***, P = 0.0001; *, P < 0.05 using Student's *t* test; ns denotes a lack of statistically significant difference.

Figure 5. **SPAT-1 links CDK-1 and PLK-1 activation for timely mitotic entry in the early *C.e.* embryo.** SPAT-1 is part of a positive feedback loop that coordinates CDK-1 and PLK-1 activation for timely mitotic entry. CyclinB/CDK-1 phosphorylates SPAT-1 to promote its interaction with PLK-1 (inactive, in closed conformation). This interaction enhances PLK-1 phosphorylation on the T loop by an activating kinase (possibly AIR-1, the Aurora A homologue in *C.e.*). Phosphorylated PLK-1 (open configuration phosphorylated at T194 residue) activates CDC-25, which dephosphorylates and thereby further activates CDK-1 (positive feedback loop). PBD, Polo box domain; K, Kinase domain; P, phosphorylation; B, CyclinB.

serine and threonine residues mutated to alanine (Fig. 4 A). We then tested the ability of the transgenes to rescue the lethality and cell division timing defects observed upon endogenous SPAT-1 depletion by RNAi (Fig. 4 B).

$GFP::spat-1^{R}$ WT transgene was able to fully rescue the lethality and the phenotypes induced by RNAi depletion of the endogenous SPAT-1 (Fig. 4, D and E). Likewise, a *GFP::spat-1* version was able to rescue the sterility phenotype of the *spat-1(tm3061)* mutant, indicating that N-terminal tagging of SPAT-1 with GFP does not alter SPAT-1 function (Fig. S2 D). We then tested SPAT-1 mutant transgenes containing either the 13 Sp/Tp sites mutated into alanine (13A) or only the N-terminally (7AN) or C-terminally located sites (6AC). All transgenes were expressed in embryos at similar levels than the control GFP::SPAT-1^{R} version (Fig. 4 C), and embryos from animals expressing these mutated proteins were viable, indicating that these versions do not act as dominant negative (Fig. 4 D). GFP::SPAT-1^{R} 13A did not rescue the embryonic lethality resulting from endogenous SPAT-1 depletion (Fig. 4 D). Likewise, a GFP::SPAT-1^{R} 7AN transgene failed to rescue endogenous SPAT-1 depletion (Fig. 4 D). In contrast, the GFP::SPAT-1^{R} 6AC transgene fully rescued *spat-1* inactivation. These results indicate that the phosphorylation sites located in the most conserved, N-terminal, part of the protein are critical for SPAT-1 function.

Close inspection of the S251 SPAT-1–bearing sequence revealed that this sequence resembles the consensus Polo docking site (F/P-F-T/Q/H/M-S-pT/pS-P/X; X, any amino acid residue; F, hydrophobic residue; Elia et al., 2003b), suggesting that phosphorylation of S251 residue might promote SPAT-1 binding to the PLK-1 PBD. Consistently, SPAT-1 interacted with the PLK-1 PBD in a yeast two-hybrid assay and in coimmunoprecipitation experiments from insect Sf9 cells and mutation of the Polo docking site (S251A) severely diminished this interaction (Fig. S2, A and B). However, *GFP::spat-1* S251A and S250A S251A transgenes rescued the sterility phenotype

of the *spat-1(tm3061)* mutant (Fig. S2 D), indicating that this site is not essential. By mutating other sites located in the N-terminal part of the protein, we found that S36, T57, and T78 are also dispensable for SPAT-1 function (Fig. 4 D). Indeed, transgenes expressing *GFP::spat-1*^{R} 4AN (S36A, T57A, T78A, and S251A) rescued lethality resulting from *spat-1* inactivation. In contrast, a *GFP::spat-1*^{R} 5AN mutant transgene containing the mutations in 4AN plus S190A resulted in 32% embryonic lethality, suggesting that S190 is important (Fig. 4 D). Consistently, a transgene expressing *GFP::spat-1*^{R} S190A similarly resulted in 22% embryonic lethality when endogenous SPAT-1 was depleted (Fig. 4 D). Likewise a *GFP::spat-1*^{R} S119A mutant transgene results in 21% embryonic lethality in the absence of endogenous SPAT-1, indicating that both S119 and S190 contribute to SPAT-1 function. We were not able to obtain transgenic lines expressing *GFP::spat-1*^{R} mutated only at T229 (mutation present in the 7AN), which prevented us from analyzing the contribution of this site to the phenotype.

We then investigated whether the embryonic lethality observed in the various mutants correlated with cell cycle timing defects. We depleted SPAT-1 by RNAi in the strains expressing GFP::SPAT-1^{R} WT and mutant transgenes and measured cell cycle length by time-lapse DIC microscopy. Consistently with the lethality data, we found that mitotic entry was only weakly delayed in embryos expressing GFP::SPAT-1^{R} 6AC and 4AN (Fig. 4 E). On the contrary, mitotic entry was strongly delayed, both in AB and P1 blastomeres, in embryos expressing GFP::SPAT-1^{R} 13A or GFP::SPAT-1^{R} 7AN protein (Fig. 4 E and Table S3). However, these embryos were not as delayed as *spat-1(RNAi)* embryos, indicating that these mutated versions retain some function in vivo. The cell cycle was also significantly delayed in embryos expressing 5AN (4AN + S190A), S119A, or S190A transgenes (Table S3).

Collectively, these results indicate that SPAT-1 phosphorylation is critical to regulate mitotic entry and that the S119 and S190 residues are important for SPAT-1 function. In the future, it will be important to study the phosphorylation kinetics of these two residues and investigate the regulatory role of multisite phosphorylation. Studies on the inactivation of the Wee1 kinase by Cdk1 in *Xenopus laevis* egg extracts have shown that this is an ultrasensitive system as a result of the competition between two sets of Cdk1 phosphorylation sites in Wee-1 (Kim and Ferrell, 2007). Given the robustness of cell division timing regulation in the *C.e.* embryo, it is tempting to speculate that a similar competition between Cdk1 phosphorylation sites may occur in SPAT-1.

In conclusion, we show that CDK-1 phosphorylates SPAT-1 to promote its interaction with PLK-1 and to trigger PLK-1 activation by Aurora A. We suggest that this is crucial to control the time of mitotic entry in the early embryo. Our results are consistent with a model in which SPAT-1 is part of a positive feedback loop that coordinates PLK-1 and CDK-1 activation (Fig. 5). Furthermore, we show that Bora phosphorylation by Cdk1 also stimulates Plk1 phosphorylation by Aurora A on its activator T loop in vitro, suggesting that the regulatory mechanism connecting Cdk1 and Plk1 activation is evolutionarily conserved.

Materials and methods

Nematode strains and culture conditions

C.e. strains were cultured and maintained using standard procedures (Brenner, 1974). Strains of the following genotypes were used: N2 and *plk-1(or683ts)* (provided by B. Bowerman, University of Oregon, Eugene, OR; O'Rourke et al., 2011). Transgenic *GFP::spat-1* WT and mutant lines were generated by microparticle bombardment of *unc-119(ed3)* mutant worms as previously described (Praitis et al., 2001) with the following modification: 20–50 µg DNA was used per transformation. Each 100-mm worm plate was bombarded twice with the same DNA construct using the Biolistic Particle Delivery System (Bio-Rad Laboratories) with a Hepta adapter. Strains generated in this study were ZU139 (unc-119(ed3) III; *[pMG897; pie-1p:GFP::spat-1 WT::pie-1 3'UTR + unc-119(+)]: GFP::spat-1*; Noatynska et al., 2010), ZU197 (unc-119(ed3) III; *[pMG871; pie-1p: GFP::spat-1^R WT::pie-1 3'UTR + unc-119(+)]: GFP::spat-1^R*), WLP398 (unc-119(ed3) III; *[pLP1247; pie-1p::GFP::spat-1^R* (S36A, T57A, T78A, S119A, S190A, T229A, S251A, T328A, S368A, T456A, T465A, S504A, T518A)::*pie1 3'UTR + unc-119(+)]: GFP::spat-1^R* 13A), WLP518 (unc-119(ed3) III; *[pMG1049; pie-1p::GFP::spat-1^R* (S36A, T57A, T78A, S119A, S190A, T229A, S251A) ::*pie-1 3'UTR + unc-119(+)]* (*GFP::spat-1^R* 7A)), WLP412 (unc-119(ed3) III; *[pLP1285; pie-1p::GFP::spat-1^R* (T328A S368A T456A T465A S504A T518A) ::*pie-1 3'UTR + unc-119(+)]* (*GFP::spat-1^R* 6AC)), ZU236 (unc-119(ed3) III; *[pMG1036; pie-1p::GFP::spat-1^R* (S36A, T57A, T78A, S251A) ::*pie-1 3'UTR + unc-119(+)]* (*GFP::spat-1^R* 4AN)), ZU243 (unc-119(ed3) III; *[pMG1040; pie-1p::GFP::spat-1^R* (S36A, T57A, T78A, S190, S251A) ::*pie-1 3'UTR + unc-119(+)]* (*GFP::spat-1^R* 5AN)), WLP416 (unc-119(ed3) III; *[pLP1287; pie-1p::GFP::spat-1^R* S190::*pie-1 3'UTR + unc-119(+)]* (*GFP::spat-1^R* S190A)), and WLP423 and WLP435 (unc-119(ed3) III; *[pLP1286; pie-1p::GFP::spat-1^R* S119::*pie-1 3'UTR + unc-119(+)]* (*GFP::spat-1^R* S119A)).

The *spat-1(tm3061)* allele was provided by S. Mitani (Tokyo Women's Medical University School of Medicine, Tokyo, Japan) and was backcrossed three times, balanced with an mnC1 balancer (Herman, 1978), and then crossed with *unc-119(ed3)* strains expressing *GFP::spat-1*-WT (strain ZU180), *GFP::spat-1* S251A (ZU203), and *GFP::spat-1* S250A S251A (ZU221). As all transgenes rescued, we were able to recover fertile homozygotes *spat-1(tm3061)* mutants.

DNA manipulation and molecular genetics

The list of plasmids used in this study is provided in Table S1. Plasmid constructions designed for yeast two-hybrid experiments, to produce recombinant MBP–SPAT-1 proteins and to generate lines expressing GFP::SPAT-1 fusion proteins, were generated by Gateway cloning according to the manufacturer's instructions (Invitrogen). The Strep tag II (IBA) was added by polymerase chain reaction. All constructs were verified by DNA sequencing (Eurofins MWG). The Bora cDNA was provided by E. Nigg (Biozentrum, Basel, Switzerland).

The SPAT-1 cDNA with the first 500 bp reencoded to be RNAi resistant was synthesized by GeneArt (Invitrogen). Amino acid substitutions were inserted by site-directed mutagenesis (QuikChange; Agilent Technologies).

RNAi

RNAi-mediated inactivation of *spat-1* was performed by injection of double-stranded RNA (dsRNA) into L4 larvae essentially as previously described (Noatynska et al., 2010). In brief, the first 494 bp of *spat-1* were amplified from *spat-1* cDNA using oligos containing T7 overhangs. dsRNA was transcribed in vitro with T7 polymerase (RiboMAX; Promega) and injected at a concentration of 0.5–1 mg/ml. *spat-1(RNAi)*–injected worms were kept at 22°C for 22 h. Partial RNAi-mediated inactivation of *cdk-1* was performed by feeding L4 larvae the bacterial clone sjj_T05G5.3 (Kamath et al., 2001) for 20 h at 20°C.

Microscopy

To measure cell cycle length, early embryos were extracted from gravid worms in egg buffer (118 mM NaCl, 48 mM KCl, 2 mM CaCl$_2$, 2 mM MgCl$_2$, and 25 mM Hepes, pH 7.3) and mounted on a 2% agarose pad. Divisions were recorded at room temperature (21°C) using a microscope (DM6000; Leica) equipped with epifluorescence and DIC optics and a camera (DFC 360 FX; Leica). Images were collected every 10 s using a 63×/1.4 NA objective and the LAS AF software (Leica). The timings of cytokinetic furrow ingression in P0 and nuclear envelope breakdown (NEBD) in AB and P1 (measured at the time of nuclear membrane disappearance) were determined. The time in seconds separating cytokinesis in P0 from NEBD in either AB or P1 corresponds to interphase. For the cell cycle analysis of the GFP::SPAT-1 transgenes, we consistently checked expression of the transgenes in each embryo that we recorded to ensure that the phenotype is not a result of loss of expression.

For worm imaging, gravid adults were incubated in M9 buffer containing 20 mM levamisole and mounted on a 2% agarose pad. Pictures were acquired on inverted microscope (Axio Observer; Carl Zeiss) using a 40× objective, equipped with DIC optics and a color camera (AxioCam HRc; Carl Zeiss). Mosaics were reconstituted by the Zen pro 2012 hardware (Carl Zeiss) using default settings.

Yeast two-hybrid analysis

Yeast two-hybrid analysis was performed using a GAL-4–based system (Gateway) in the PJ69-4A yeast strain (MATa *trp1-901 leu2-3, 112 ura3-52 his3-200 gal4(D) gal80(D)* LYS2::GAL1-HIS3 GAL2-ADE2 met2::GAL7-lacZ; James et al., 1996) expressing as bait the PLK-1 PBD (C-terminal 309 amino acids of PLK-1; Noatynska et al., 2010) and full-length SPAT-1 WT, SPAT-1 S251A, or S251D as preys. Transformed clones hosting the prey bait–positive interaction were selected on selective medium lacking leucine, tryptophan, and histidine and containing 25 mM 3AT drug (3-amino-1, 2, 4-triazole; Sigma-Aldrich). Nine independent colonies were tested for each interaction.

Protein purification and coimmunoprecipitation

MBP and MBP–SPAT-1 fusion proteins were expressed in *Escherichia coli* BL21 DE3 pLysS (Invitrogen) strain and purified on amylose resin according to the manufacturer's instructions (New England Biolabs, Inc.). In brief, MBP–SPAT-1 expression was induced by addition of 1 mM isopropyl β-D-thiogalactopyranoside (Sigma-Aldrich) to 1 liter of Terrific Broth culture of BL21 cells before incubation overnight at 18°C. After centrifugation, the bacteria were resuspended in 20 ml lysis buffer (20 mM Hepes, pH 7.4, 200 mM NaCl, 2 mM DTT, and 1 mM EDTA) and lysed with a homogenizer (EmulsiFlex; Avestin). The soluble portion of the lysate was incubated with amylose resin. The resin was washed with 10 volumes of lysis buffer, and bound proteins were eluted in lysis buffer containing 20 mM maltose (Sigma-Aldrich).

Recombinant proteins expressed in insect Sf9 cells were produced with the Bac-to-Bac Baculovirus Expression System according to the manufacturer's instructions (Invitrogen). Baculoviruses expressing the *C.e.* PBD in fusion with GST were a gift from T. Hyman (Max Planck Institute of Molecular Cell Biology and Genetics, Dresden, Germany; Decker et al., 2011).

To produce *C.e.* 6×(His)–PLK-1 WT and *C.e.* 6×(His)–PLK-1 T194A, insect Sf9 cells were infected with appropriate baculovirus and then lysed in lysis buffer (PBS, pH 7.2, 250 mM NaCl, 30 mM imidazole, and protease and phosphatase inhibitors [Roche]) by passing the cell suspension 30 times through a 21-gauge syringe needle. The lysate was clarified by centrifugation for 10 min at 16,000 *g*, and the supernatant was injected on HiTrap Chelating HP column loaded with nickel sulfate (GE Healthcare). Proteins were eluted by an imidazole gradient using a fast protein LC Äkta System (GE Healthcare). Most purified elution fractions were pooled, diluted volume to volume in the lysis buffer without imidazole and containing 50% glycerol, concentrated on a centrifugal concentrator (Vivaspin VS15RH12; Vivaproducts), flash frozen in liquid nitrogen, and stored at −80°C.

For proteins used in Figs. 1 D and 2 (C–F), 5.3 × 10^6 insect Sf9 cells were plated in 6-well plates and infected or coinfected with the appropriate combination of viruses and incubated at 27°C for 72 h. Cells were then lysed in 300 µl lysis buffer (PBS, pH 7.2, 250 mM NaCl, and protease inhibitors [Roche]) by passing the cell suspension 30 times though a 21-gauge syringe needle. The lysate was clarified by centrifugation for 10 min at 16,000 *g*, and the supernatant was incubated with 50 µl Strep-Tactin Sepharose beads or 25 µl glutathione–Sepharose 4B beads (GE Healthcare). The beads were washed five times and used for subsequent experiments. In the case of GST-tagged proteins, elution was performed with 3× Laemmli buffer (Fig. S2).

For the PLK-1 pull-down assay presented in Figs. 1 D and 2 E, an extract of insect Sf9 cells expressing 6×(His)–PLK-1 was incubated on Strep-Tactin Sepharose beads coupled to Strep–SPAT-1 WT or mutant, dephosphorylated by λ phosphatase (see Phosphatase treatment section), and rephosphorylated or not rephosphorylated by *H.s.* CyclinB/Cdk1 (see Kinase assays section) during 1 h at 4°C. The beads were then washed five times, and proteins were eluted with 5 mM desthiobiotin and analyzed by SDS-PAGE and Western blotting.

For immunoprecipitation experiments of PLK-1 from embryonic extract, worms were grown in liquid culture, and embryos were harvested from gravid worms by bleaching (500 mM NaOH and 15% bleach). Packed embryos were frozen in liquid nitrogen and stored at −80°C. Embryos

were then thawed, resuspended in immunoprecipitation buffer (100 mM KCl, 50 mM Tris, pH 7.5, 1 mM MgCl$_2$, 1 mM DTT, 5% glycerol, 0.05% NP-40, 1 mM EDTA, and protease and phosphatase inhibitor cocktail [Roche]), and frozen in liquid nitrogen. The embryos were ground on dry ice using a mortar and pestle. The protein homogenate was thawed on ice and centrifuged at 13,000 rpm for 30 min at 4°C. 450 µg protein was incubated at 4°C for 1 h with 10 mg of either PLK-1 or IgG antibody. Next, 15 µl protein A beads was added to each tube for 30 min at 4°C. The beads were washed five times with immunoprecipitation buffer and boiled with SDS sample buffer.

Gel filtration analysis of SPAT-1
Strep–SPAT-1 WT and Strep–SPAT-1 13A proteins produced in insect Sf9 cells were captured on Strep-Tactin Sepharose beads, dephosphorylated with λ phosphatase (see Phosphatase treatment section), and eluted in PBS buffer, pH 7.2, and 250 mM NaCl containing 5 mM desthiobiotin. Eluted proteins were centrifuged for 10 min at 16,000 *g*, and 100 µl was injected on a Superdex 200 10/300 GL column (GE Healthcare) equilibrated in PBS, pH 7.2, and 250 mM NaCl at a flow rate of 0.5 ml/min on a fast protein LC Äkta System. The column was calibrated using a Gel Filtration calibration kit (Sigma-Aldrich), which contains a mixture of five different proteins (669-kD thyroglobulin, 443-kD apoferritin, 200-kD β-amylase, 150-kD alcohol dehydrogenase, and 29-kD carbonic anhydrase).

Biochemical assays
Phosphatase treatment. Dephosphorylation of immobilized Strep–SPAT-1 WT or mutants on Strep-Tactin Sepharose beads was performed for 2 h in λ phosphatase buffer supplemented with MnCl$_2$ and 400 U λ phosphatase (New England Biolabs, Inc.). Then, λ phosphatase was washed away, and subsequent steps were performed in the presence of phosphatase inhibitors (Figs. 1 D and 2 E).

Kinase assays. CyclinB/Cdk1-dependent kinase assays were performed in Cdk1 kinase buffer (50 mM Hepes, pH 7.6, 10 mM MgCl$_2$, 1 mM DTT, and protease and phosphatase inhibitors [Roche]) with 20 U *H.s.* CyclinB/Cdk1 (New England Biolabs, Inc.) in a final volume of 30 µl containing either 300 ng full-length MBP–SPAT-1 or MBP (Figs. 1 B, 3, and S1) or immobilized Strep–SPAT-1 on Strep-Tactin Sepharose beads (Figs. 1 D and 2, C and E). Reactions were initiated by adding a mix of 0.2 mM ATP and, in the specific cases of Figs. 1 B and 2 C, 5 µCi γ-[³²P]ATP (PerkinElmer), during 40 min at 30°C. For these experiments, samples were boiled in Laemmli buffer 3× and visualized by Coomassie blue staining, γ-[³²P]ATP incorporation was analyzed with a phosphorimager (LAS 4000; GE Healthcare).

Aurora A–dependent kinase assays were performed in Aurora A kinase buffer (50 mM Tris, pH 7.5, 15 mM MgCl$_2$, 2 mM EGTA, 1 mM DTT, and protease and phosphatase inhibitors [Roche]) in a final volume of 30 µl with 375 ng of 6×(His)–PLK-1 (this study) or 6×(His)–Plk1 (EMD Millipore), 500 ng *H.s.* 6×(His)–Aurora A (Invitrogen), and 500 ng MBP or MBP–SPAT-1 phosphorylated or not phosphorylated by *H.s.* CyclinB/Cdk1. Reactions were initiated by adding a mix of 0.2 mM ATP for 40 min at 30°C. Samples were boiled in Laemmli buffer 3× and analyzed by Western blotting.

Western blotting and antibodies
Western blot analysis was performed using standard procedures (Sambrook et al., 1989). For PLK-1 antibodies, the C-terminal 180 bp of PLK-1 was cloned into pDEST15 using Gateway technology (Life Technologies), and the purified GST fusion protein was injected into rabbits. The serum was purified on a MBP–PLK-1 column and used at 1:1,000 for the described experiments. Other antibodies include SPAT-1 (rabbit; 1:1,000; Noatynska et al., 2010), MBP (1:1,000; mouse; New England Biolabs, Inc.), Tubulin 1:1,000 (mouse, DM1a; Sigma-Aldrich), Actin (1:1,000; mouse, clone C4; MP Biomedicals), Plk1 pT210 (1:1,000; rabbit; Cell Signaling Technology), and phospho-Ser (Cdks) substrate (1:1,000; rabbit; Cell Signaling Technology). HRP-conjugated anti–mouse and anti–rabbit antibodies (Sigma-Aldrich) were used at 1:3,000, and the signal was detected with chemiluminescence (Thermo Fisher Scientific).

Identification of SPAT-1 phosphorylation sites by LC-MS/MS
For the analysis of SPAT-1 phosphorylated in vitro (Fig. 2 A), the protein mixture containing MBP–SPAT-1 phosphorylated by CyclinB/Cdk1 was digested overnight at 37°C using sequencing grade trypsin (12.5 µg/ml; Promega) in 20 µl of 25-mmol/liter NH$_4$HCO$_3$. Digests were analyzed by a LTQ Velos Orbitrap (Thermo Fisher Scientific) coupled to an Easy nano-LC Proxeon system (Thermo Fisher Scientific). An Easy column Proxeon

C18 (2 cm, 100 µm inner diameter, and 120 A) was used for peptide preconcentration and an Easy Column Proxeon C18 (10 cm, 75 µm inner diameter, and 120 A) for peptide separation. Chromatographic separation of the peptides was performed with the following parameters: 300 nl/min flow, gradient rising from 95% solvent A (water–0.1% formic acid) to 25% B (100% acetonitrile and 0.1% formic acid) in 20 min and then to 45% B in 40 min and finally to 80% B in 10 min. Peptides were analyzed in the Orbitrap in full ion scan mode at a resolution of 30,000 (at mass per charge of 400), a mass range of mass per charge of 400–1,800. Fragments were obtained with a collision-induced dissociation activation energy of 35% and an activation Q of 0.250 for 10 ms and analyzed in the LTQ in a second scan event. The maximum ion accumulation times were set to 100 ms for MS acquisition and 50 ms for MS/MS acquisition. MS/MS data were acquired in a data-dependent mode in which the 20 most intense precursor ions were isolated, with a dynamic exclusion of 20 s, an exclusion mass width of 10 ppm, an exclusion list size of 500, and a repeat duration of 30 s.

For the analysis of SPAT-1 phosphorylation sites in vivo (Fig. 2 A), SPAT-1 or GFP::SPAT-1 was captured from embryo extracts using SPAT-1 antibodies (Noatynska et al., 2010) or GFP nanobodies (Rothbauer et al., 2008; ChromoTek), respectively. The beads carrying the immune complexes were washed with binding buffer and then rinsed with 100 µl of 25-mmol/liter NH$_4$HCO$_3$. Proteins on beads were digested overnight at 37°C using sequencing grade trypsin (12.5 µg/ml) in 20 µl of 25-mmol/liter NH$_4$HCO$_3$. The same chromatographic, MS conditions, and data analysis parameters as described in the previous paragraph were used.

Improvement of phosphosites detection from in vivo phosphorylated SPAT-1. To improve the sensitivity for the phosphorylated peptides of SPAT-1 found in vitro and not directly detected in vivo analysis, the following parameters were used for inclusion list-dependent acquisition on the Orbitrap mass spectrometer: the ion trap MS/MS max ion time was increased to 200 ms. Five scan events were acquired continuously on 18 precursors corresponding to 13 phosphorylation sites found in vitro, which were targeted for MS/MS spectrum acquisition: peptide MH$_3$³⁺ (617.31 TAEWKVpSPIAAERPSK (S36)), peptide MH$_2$²⁺ (691.33 NVSYIPpSPDGPR (S190)), peptide MH$_2$²⁺ (605.80 LFSAGGpTPGAPR (T328)), peptide MH$_2$²⁺ (604.28 SlpTPQQNDPK (T78)), peptide MH$_2$²⁺ (756.87 AYApTSSPKQRPR (S251)), peptide MH$_2$²⁺ (493.24685 SGFKpTPLR (T57)), peptide MH$_3$³⁺ (921.07859 SINTTDPST-SGYDSKSIpTPQQNDPK (T78)), peptide MH$_2$²⁺ (450.70163 SINFpSPR (S119)), peptide MH$_4$⁴⁺ (1,105.52948 YINLSHRDGTVTTFTYGAEEN-ATSSSAPGAAAGtPASLANIVR (T229)), peptide MH$_4$⁴⁺ (884.66222 DGT-VTTFTYGAEENATSSSAPGAAAGpTPASLANIVR (T229)), peptide MH$_3$³⁺ (456.22603 RLFSAGGpTPGAPR (T328)), peptide MH$_4$⁴⁺ (1,119.71924 DDEDEADDVENSSMLSNDDLMLNETNGQHFNDSLpSPVRK (S368)) peptide MH$_3$³⁺ (712.64157 SSSSNApTPRHEDLDWTPR (T456)), peptide MH$_2$²⁺ (1108.44021 SSSSNApTPRHEDLDWpTPR (T456, T465)), peptide MH$_3$³⁺ (416.83972 HEDLDWpTPR (T465)), peptide MH$_4$⁴⁺ (594.27411 RFVFDMpSPIHPNHNAPGAMR (S504)), peptide MH$_3$³⁺ (739.99616 FVFDMpSPIHPNHNAPGAMR (S504)), and peptide MH$_3$³⁺ (938.44461 FVFDMSPIHPNHNAPGAMRpTPLQR (T518)).

Data processing of MS analysis. Data were processed with Proteome Discoverer 1.4 software (Thermo Fisher Scientific) coupled to an in-house Mascot search server (version 2.4.1; Matrix Science). The mass tolerance of fragment ions was set to 7 ppm for precursor ions and 0.5 D for fragments. The following modifications were used in variable modifications: oxidation (M) and phosphorylations (STY). Phosphorylation localizations were evaluated by the Phospho-RS 3.1 algorithm (Taus et al., 2011). The maximum number of missed cleavages was limited to 2 for trypsin digestion. MS–MS data were searched against the NCBI-nr (nonredundant) database with the *C.e.* taxonomy. The false discovery rate was calculated using the support vector machine–based algorithm Percolator with a 5% q-value in relaxed mode and 1% q-value in stringent mode was used. A threshold of 1% was chosen for this rate.

Online supplemental material
Fig. S1 documents control experiments relevant to Fig. 3 (phosphorylation of PLK-1/Plk1 is strictly dependent on Aurora A). Fig. S2 shows the lack of interaction of the Polo docking site mutant (SPAT-1 S251A) with the PBD of PLK-1 but the ability of this mutant and the double (SPAT-1 S250A and S251A) mutant to rescue the sterility of *spat-1(tm3061)* mutant animals. Table S1 is the list of plasmids used in this study. Table S2 shows the MS data presented in Fig. 2 and is provided online as an Excel (Microsoft) file. Table S3 documents the statistics relatives to Fig. 4 and is provided online as an Excel file. Online supplemental material is available at http://www.jcb.org/cgi/content/full/jcb.201408064/DC1.

References

Archambault, V., and D.M. Glover. 2009. Polo-like kinases: conservation and divergence in their functions and regulation. *Nat. Rev. Mol. Cell Biol.* 10:265–275. http://dx.doi.org/10.1038/nrm2653

Brenner, S. 1974. The genetics of *Caenorhabditis elegans*. *Genetics*. 77:71–94.

Bruinsma, W., J.A. Raaijmakers, and R.H. Medema. 2012. Switching Polo-like kinase-1 on and off in time and space. *Trends Biochem. Sci.* 37:534–542. http://dx.doi.org/10.1016/j.tibs.2012.09.005

Budirahardja, Y., and P. Gönczy. 2008. PLK-1 asymmetry contributes to asynchronous cell division of *C. elegans* embryos. *Development*. 135:1303–1313. http://dx.doi.org/10.1242/dev.019075

Chan, E.H., A. Santamaria, H.H. Silljé, and E.A. Nigg. 2008. Plk1 regulates mitotic Aurora A function through betaTrCP-dependent degradation of hBora. *Chromosoma*. 117:457–469. http://dx.doi.org/10.1007/s00412-008-0165-5

Chase, D., C. Serafinas, N. Ashcroft, M. Kosinski, D. Longo, D.K. Ferris, and A. Golden. 2000. The polo-like kinase PLK-1 is required for nuclear envelope breakdown and the completion of meiosis in *Caenorhabditis elegans*. *Genesis*. 26:26–41. http://dx.doi.org/10.1002/(SICI)1526-968X(200001)26:1<26::AID-GENE6>3.0.CO;2-O

Decker, M., S. Jaensch, A. Pozniakovsky, A. Zinke, K.F. O'Connell, W. Zachariae, E. Myers, and A.A. Hyman. 2011. Limiting amounts of centrosome material set centrosome size in *C. elegans* embryos. *Curr. Biol.* 21:1259–1267. http://dx.doi.org/10.1016/j.cub.2011.06.002

Deppe, U., E. Schierenberg, T. Cole, C. Krieg, D. Schmitt, B. Yoder, and G. von Ehrenstein. 1978. Cell lineages of the embryo of the nematode *Caenorhabditis elegans*. *Proc. Natl. Acad. Sci. USA*. 75:376–380. http://dx.doi.org/10.1073/pnas.75.1.376

Elia, A.E., L.C. Cantley, and M.B. Yaffe. 2003a. Proteomic screen finds pSer/pThr-binding domain localizing Plk1 to mitotic substrates. *Science*. 299:1228–1231. http://dx.doi.org/10.1126/science.1079079

Elia, A.E., P. Rellos, L.F. Haire, J.W. Chao, F.J. Ivins, K. Hoepker, D. Mohammad, L.C. Cantley, S.J. Smerdon, and M.B. Yaffe. 2003b. The molecular basis for phosphodependent substrate targeting and regulation of Plks by the Polo-box domain. *Cell*. 115:83–95. http://dx.doi.org/10.1016/S0092-8674(03)00725-6

Herman, R.K. 1978. Crossover suppressors and balanced recessive lethals in *Caenorhabditis elegans*. *Genetics*. 88:49–65.

Hutterer, A., D. Berdnik, F. Wirtz-Peitz, M. Zigman, A. Schleiffer, and J.A. Knoblich. 2006. Mitotic activation of the kinase Aurora-A requires its binding partner Bora. *Dev. Cell*. 11:147–157. http://dx.doi.org/10.1016/j.devcel.2006.06.002

James, P., J. Halladay, and E.A. Craig. 1996. Genomic libraries and a host strain designed for highly efficient two-hybrid selection in yeast. *Genetics*. 144:1425–1436.

Kamath, R.S., M. Martinez-Campos, P. Zipperlen, A.G. Fraser, and J. Ahringer. 2001. Effectiveness of specific RNA-mediated interference through ingested double-stranded RNA in *Caenorhabditis elegans*. *Genome Biol.* 2:H0002.

Kim, S.Y., and J.E.J. Ferrell Jr. 2007. Substrate competition as a source of ultrasensitivity in the inactivation of Wee1. *Cell*. 128:1133–1145. http://dx.doi.org/10.1016/j.cell.2007.01.039

Macůrek, L., A. Lindqvist, D. Lim, M.A. Lampson, R. Klompmaker, R. Freire, C. Clouin, S.S. Taylor, M.B. Yaffe, and R.H. Medema. 2008. Polo-like kinase-1 is activated by aurora A to promote checkpoint recovery. *Nature*. 455:119–123. http://dx.doi.org/10.1038/nature07185

Nishi, Y., E. Rogers, S.M. Robertson, and R. Lin. 2008. Polo kinases regulate *C. elegans* embryonic polarity via binding to DYRK2-primed MEX-5 and MEX-6. *Development*. 135:687–697. http://dx.doi.org/10.1242/dev.013425

Noatynska, A., C. Panbianco, and M. Gotta. 2010. SPAT-1/Bora acts with Polo-like kinase 1 to regulate PAR polarity and cell cycle progression. *Development*. 137:3315–3325. http://dx.doi.org/10.1242/dev.055293

O'Rourke, S.M., C. Carter, L. Carter, S.N. Christensen, M.P. Jones, B. Nash, M.H. Price, D.W. Turnbull, A.R. Garner, D.R. Hamill, et al. 2011. A survey of new temperature-sensitive, embryonic-lethal mutations in *C. elegans*: 24 alleles of thirteen genes. *PLoS ONE*. 6:e16644. http://dx.doi.org/10.1371/journal.pone.0016644

Praitis, V., E. Casey, D. Collar, and J. Austin. 2001. Creation of low-copy integrated transgenic lines in *Caenorhabditis elegans*. *Genetics*. 157:1217–1226.

Rivers, D.M., S. Moreno, M. Abraham, and J. Ahringer. 2008. PAR proteins direct asymmetry of the cell cycle regulators Polo-like kinase and Cdc25. *J. Cell Biol.* 180:877–885. http://dx.doi.org/10.1083/jcb.200710018

Rothbauer, U., K. Zolghadr, S. Muyldermans, A. Schepers, M.C. Cardoso, and H. Leonhardt. 2008. A versatile nanotrap for biochemical and functional studies with fluorescent fusion proteins. *Mol. Cell. Proteomics*. 7:282–289. http://dx.doi.org/10.1074/mcp.M700342-MCP200

Sambrook, J., E.F. Fritsch, and T. Maniatis. 1989. Molecular cloning: a laboratory manual. Second edition. Cold Spring Harbor Laboratory Press, Cold Spring Harbor, NY. 626 pp.

Seki, A., J.A. Coppinger, C.Y. Jang, J.R. Yates, and G. Fang. 2008. Bora and the kinase Aurora a cooperatively activate the kinase Plk1 and control mitotic entry. *Science*. 320:1655–1658. http://dx.doi.org/10.1126/science.1157425

Sulston, J.E., E. Schierenberg, J.G. White, and J.N. Thomson. 1983. The embryonic cell lineage of the nematode *Caenorhabditis elegans*. *Dev. Biol.* 100:64–119. http://dx.doi.org/10.1016/0012-1606(83)90201-4

Taus, T., T. Köcher, P. Pichler, C. Paschke, A. Schmidt, C. Henrich, and K. Mechtler. 2011. Universal and confident phosphorylation site localization using phosphoRS. *J. Proteome Res.* 10:5354–5362. http://dx.doi.org/10.1021/pr200611n